Hydrology and Earth System Sciences Discussions

Evaluation of high-resolution satellite precipitation products using rain gauge observations over the Tibetan Plateau

Y. C. Gao[1] and M. F. Liu[1,2]

[1]Institute of Geographical Sciences and Natural Resources Research, Chinese Academy of Sciences, P.O. Box 9719, Beijing, 100101, China
[2]Graduate School of the Chinese Academy of Sciences, Beijing, 100039, China

Correspondence to: M. F. Liu (vanni05@gmail.com)

HESSD

9, 9503–9532, 2012

Evaluation of high-resolution satellite precipitation products

Y. C. Gao and M. F. Liu

Title Page

Abstract · Introduction

Conclusions · References

Tables · Figures

◁ · ▷

◀ · ▶

Back · Close

Full Screen / Esc

Printer-friendly Version

Interactive Discussion

Abstract

High-resolution satellite precipitation products are very attractive for studying the hydrologic processes in mountainous areas where rain gauges are generally sparse. Three high-resolution satellite precipitation products are evaluated using gauge measurements over different climate zones of the Tibetan Plateau (TP) within a 6 yr period from 2004 to 2009. The three satellite-based precipitation datasets are: Tropical Rainfall Measuring Mission (TRMM) Multisatellite Precipitation Analysis (TMPA), Climate Prediction Center Morphing Technique (CMOPRH) and Precipitation Estimation from Remotely Sensed Information using Artificial Neural Network (PERSIANN). TMPA and CMORPH, with higher correlation coefficients and lower root mean square errors (RMSEs), show overall better performance than PERSIANN. TMPA has the lowest biases among the three precipitation datasets, which is likely due to the correction process against monthly gauge observations from global precipitation climatology project (GPCP). The three products show better agreement with gauge measurements over humid regions than that over arid regions where correlation coefficients are less than 0.5. Moreover, the three precipitation products generally tend to overestimate light rainfall (0–10 mm) and underestimate moderate and heavy rainfall (> 10 mm). PERSIANN produces obvious underestimation at low elevations and overestimation at high elevations. CMORPH and TMPA do not present strong bias-elevation relationships in most regions of TP.

1 Introduction

The Tibetan Plateau (TP) is one of the highest plateaus in the world with an average altitude of 4000 m above the sea level and an area of about 2.4 million km^2. TP is the water source area of some important rivers (e.g. Yangzte, Yellow, Lancang-Mekong, Salween-Nujiang and Brahmaputra), which greatly affect hundreds of millions of people lived in China. TP has a significant thermal difference from its peripheral areas,

known as heating source in the summer and cooling source in the winter, which has a far-reaching impact on the Asian monsoon systems and the formation of the East China climate (Yeh and Gao, 1979; Yanai et al., 1992). Wang et al. (2003) found that the evolution and eastward motion of convective cloud systems over TP played impor-

5 tant roles in the development and strengthening of rainstorms in the Yangtze River in 1998. Note that the 1998 severe flood event in the Yangtze River killed thousands of people and destroyed about seven million houses. Shi et al. (2008) further found that the mesoscale feature in topography enhanced mesoscale disturbances over TP, which propagated eastward and caused the increase of precipitation in the Yangtze River in

10 1998. Understanding the meteorological variations and hydrological processes of TP cannot be overemphasized. Yang et al. (2011) suggested that observed precipitation showed insignificant increasing trend over central TP and decreasing trends along the TP periphery. However, their results are based on rain gauges and may loss the representativeness due to the low gauge density over TP. Thus, it is important to explore

15 accurate documentation of the temporal and spatial distribution of precipitation.

The development of remote sensing technology has brought unprecedented opportunity to estimate precipitation by using radiometric observations. They can be classified into two main groups (Sapiano and Arkin, 2009). (1) Infrared (IR) imagery, which benefits from the high sampling frequency but yields crude estimates of precipita-

20 tion because of the indirect relationship between cloud-top temperature and precipitation. (2) Microwave (MW), which tends to produce more accurate precipitation retrievals due to the direct connection with rainfall, but suffers from infrequent temporal sampling problem. Recently, several high-resolution precipitation products (0.25° and 3 hourly) by merging MW and IR data have emerged, such as Precipitation Estima-

25 tion from Remotely Sensed Information using Artificial Neural Networks (PERSIANN; Hsu et al., 1999; Sorooshian et al., 2000), Climate Prediction Center Morphing Method (CMORPH; Joyce et al., 2004), and TRMM Multisatellite Precipitation Analysis (TMPA; Huffman et al., 2007). They have been used in many different ways such as climate

Evaluation of high-resolution satellite precipitation products

Y. C. Gao and M. F. Liu

Title Page

Abstract	Introduction
Conclusions	References
Tables	Figures

◄◄ ►►

◄ ►

Back Close

Full Screen / Esc

Printer-friendly Version

Interactive Discussion

studies and hydrological analysis (e.g. Gottschalck et al., 2005; Shi et al., 2008; Pan et al., 2010).

High-resolution precipitation products provide a strong basis for studying the hydrologic processes in large mountainous areas. However, the accuracies of these products need to be validated. There have been several studies focusing on the evaluation of the performance of high-resolution precipitation products over mountainous regions. Hong et al. (2007) compared PERSIANN-CCS (an improved version of PERSIANN; Hong et al., 2004) rainfall estimation with rain gauge observations in a complex terrain region of northwestern Mexico. They reported that PERSIANN-CCS tended to underestimate the occurrence of light precipitation at high elevation and to overestimate the occurrence of precipitation in low elevation, resulting in an overall positive bias in PERSIANN-CCS. In Ethiopia, Hirpa et al. (2010) evaluated three high-resolution precipitation products over complex terrain at annual time scale and found that PERSIANN could not show the elevation-dependent trend exhibited in TMPA 3B42RT (the real-time version without correction against gauge observations), CMORPH and gauge measurements. The superiority of MW-based TMPA 3B42 and CMORPH to IR-based PERSIANN over Ethiopia has also been validated by Dinku et al. (2008) at daily scale and Romilly and Gebremichael (2011) at monthly scale. Romilly and Gebremichael (2011) indicated that the impact of elevation on the performance of satellite estimates must be region specific. Sorooshian et al. (2011) also recommended that error properties of satellite-based precipitation should be studied in different climate regions and altitudes.

Yin et al. (2008) built a topography-based correction method for satellite-based precipitation estimates and found that TRMM 3B42 version 5 (an earlier version of TMPA) generated consistent overestimation over TP at monthly time scale. They also reported obvious improvements over 3B42 version 5 when considering the performance of TRMM 3B43 version 6 that incorporated more MW data including the Special Sensor Microwave Imager (SSM/I) and Advanced Microwave Sounding Unit (AMSU). However, their study was confined to monthly rainfall while hydrological process studies are generally at least based on daily scale. Our study focuses on the evaluation of three widely

Evaluation of high-resolution satellite precipitation products

Y. C. Gao and M. F. Liu

Title Page

Abstract | Introduction

Conclusions | References

Tables | Figures

|◀ | ▶|

◀ | ▶

Back | Close

Full Screen / Esc

Printer-friendly Version

Interactive Discussion

used satellite-based precipitation products over TP at daily time scale and the impact of elevation on satellite estimates is examined in specific climate zones. The performance of the satellite precipitation estimates is expected to provide suggestions for the application of these precipitation products over TP.

This paper is organized as follows: Sect. 2 provides a description of datasets and method; Sect. 3 discusses the comparison between high-resolution satellite precipitation datasets and rain gauge observations, and a summary is given in Sect. 4.

2 Data and method

2.1 Study area

TP is located in the northwestern China, including Xizang (Tibet), Qinghai, Gansu, southern Xinjiang and western Sichuan province. Our study mainly focuses on the area of 25–40° N and 75–105° E with mean elevation of about 4292 m (Fig. 1). Topography plays an important role in creating disparate microclimates ranging from deserts to forests. For example, the average elevation of Qaidam basin is largely lower than peripheral regions, which prevents water vapor from flowing into the basin to form rainfall and leads to its being an extremely arid area. Sun and Zheng (1999) divided TP and its peripheral regions into zones according to climatic factors shown in Table 1 (Fig. 2). For example, the Qaidam basin is located in the zone of HIID1 characterized as a temperate and arid zone. Table 2 presents mean elevation, six-year mean rainy season precipitation and the number of rain gauges within every zone. Arid zones generally receive rainfall less than 150 mm while humid zones receive more than 600 mm except zone IVA. Note that three satellite products are used to roughly assign the rainy season precipitation because they can provide continuous coverage. However, it is worth noting that they are all biased and will be evaluated later.

Title Page

Abstract	Introduction
Conclusions	References
Tables	Figures

◀ | ▶

◀ | ▶

Back | Close

Full Screen / Esc

Printer-friendly Version

Interactive Discussion

2.2 Satellite precipitation data

Three high-resolution precipitation products PERSIANN, TMPA 3B42 version 6 and CMORPH that map global precipitation at 3-hourly and 0.25° resolution are examined in our study. A good and detailed description of them and their inputs are available in Sapiano and Arkin (2009). We here only briefly summarize the algorithms for re-trieving rainfall. In the PERSIANN algorithm, an artificial neural network is used to train IR-precipitation relationship with TRMM Microwave Imager (TMI) and other MW data (Hsu et al., 1999; Sorooshian et al., 2000). The trained network is then applied to determine precipitation estimates based on IR measurements. TMPA establishes IR-precipitation relationship by matching the probability density function between MW precipitation retrievals and IR observations (Huffman et al., 2007). MW estimates are preferentially used when MW data are available, and IR estimates are used to fill the grids that are not covered by MW retrievals. The combined precipitation estimates are then calibrated and rescaled using the GPCP monthly gauge data over land (Huffman et al., 1997). Based on IR measurements, CMORPH constructs motion vectors of cloud systems to interpolate the infrequent MW estimates with time to create consistent time series for precipitation (Joyce et al., 2004).

2.3 Rain gauge data

We collect a surface precipitation dataset from the National Meteorological Informa-tion Center of the China Meteorological Administration (CMA). The dataset consists of daily precipitation records during 2004–2009 at 166 rain gauges located in central TP and its peripheral areas (Fig. 1). A strict quality control process has been applied by CMA to check and validate extreme values. Wind and snow can cause inaccura-cies to rain gauge observations (Legates and Willmott, 1990). Therefore, our study only refers to summer and fall seasons from May to October. It is worth noting that the selected months cover rainy seasons and the accumulated precipitation in these months account for 86.8 % of the annual precipitation from 2004 to 2009. Note that the

accumulated and annual precipitation is simply calculated as the mean value of the 166 gauge measurements over TP.

It is not possible to reach perfect spatial matching between point measurements from gauges and spatially averaged estimates from satellite products (Hong et al., 2007; Sapiano and Arkin, 2009; Hirpa et al., 2010; Romilly and Gebremichael, 2011). Fundamental difficulties exist when comparing gauge measurements and satellite estimates: retrieval errors of satellite algorithms, sampling errors caused by different sampling schemes, systematic gauge errors related to instruments, etc. (Ciach and Krajewski, 1999; Bowman, 2005). However, this study is not aimed to precisely quantify the errors of satellite estimates in individual rain events, but to evaluate the overall performance of the three satellite products over a long period and its relationship to local climate and topography. Moreover, we cover a period of 6 yr (2004–2009) to create large rainfall samples that are expected to relieve the interference of sampling errors. Xie et al. (2007) constructed a gridded daily precipitation dataset based on gauge observations over East Asia. The gridded dataset performed well over most regions of China except over TP. The sparse gauge network of TP did not allow accurate estimation of analyzed precipitation field. In order to avoid large inaccuracies caused by up-scaling interpolation, we follow a downscaling method used by Sapiano and Arkin (2009) that builds the matched rainfall series for each gauge station by combining the surrounding four grids points from the satellite analyses using bilinear interpolation. By integrating the nearest four grids instead of the single grid that contains rain gauge, we expect to relieve errors caused by wind and other spatial sampling problems (Bell and Kundu, 2003; Bowman, 2005). Moreover, Demirtas et al. (2005) compared two types of verification techniques for model precipitation forecasts: "grid-to-grid" and "grid-to-point" with bilinear interpolation and found that the two methods led to similar conclusions. The 3-hourly precipitation in the satellite datasets is accumulated to daily rainfall following the method used in Shen et al. (2010). It should be noted that the three satellite products with Universal Time Coordinated (UTC) have been transformed to Local Standard Time (LST) to be consistent with rain gauges.

Evaluation of high-resolution satellite precipitation products

Y. C. Gao and M. F. Liu

Full Screen / Esc

Printer-friendly Version

Interactive Discussion

Discussion Paper | Discussion Paper | Discussion Paper | Discussion Paper

2.4 Statistical indices

To quantitatively compare satellite products with rain gauge measurements, a set of statistics are used in our study: correlations, bias and root mean square errors (RMSE). To detect the satellite's ability of delineating rain/no rain events, we also adopt a set of contingency table statistics: probability of detection (POD) that measures the ratio of rain occurrences correctly detected to the total number of observed events, false alarm ratio (FAR) that measures the ratio of the number of falsely alarmed rain events to the total number of detected events, and equitable threat score (ETS) that is modified to account for hits due to random chance (Schaefer, 1990; Ebert et al., 2007). Note that all the statistics are calculated based on time series of gauge points created by the previously mentioned downscaling method. The equations of these statistics are shown below.

$$\text{Correlation} = \frac{\sum_{i=1}^{n} \left(G_i - \overline{G}\right)\left(S_i - \overline{S}\right)}{\sqrt{\sum_{i=1}^{n} \left(G_i - \overline{G}\right)^2} \times \sqrt{\sum_{i=1}^{n} \left(S_i - \overline{S}\right)^2}}. \tag{1}$$

$$\text{Bias} = \frac{1}{n} \sum_{i=1}^{n} (S_i - G_i). \tag{2}$$

$$\text{Relative bias} = \frac{\sum_{i=1}^{n} (S_i - G_i)}{\sum_{i=1}^{n} G_i}. \tag{3}$$

$$\text{RMSE} = \sqrt{\frac{1}{n} \sum_{i=1}^{n} (S_i - G_i)^2}. \tag{4}$$

$$POD = \frac{H}{H + M}. \tag{5}$$

$$FAR = \frac{F}{H + F}. \tag{6}$$

$$ETS = \frac{H - H_e}{H + M + F - H_e}. \tag{7}$$

where, G_i mean gauge observations and $\overline{G}$ is the average of gauge observations. S_i and $\overline{S}$ are satellite estimates and their average, respectively. H: observed rain correctly detected; M: observed rain not detected; F: rain detected but not observed; $H_e = (H + M)(H + F)/N$ and N is the total number of estimates. Detailed information about contingency table statistics can be referred to Ebert et al. (2007).

3 Results and discussion

3.1 Spatial precipitation patterns of satellite datasets

Figure 3 shows the spatial distribution of six-year mean rainy season precipitation over TP and its peripheral areas. All three satellite datasets present an increasing trend of precipitation from northwest to southeast over TP. They clearly reveal small precipitation amount in Tarim basin (37–40° N and 80–90° E, mainly located in zone IIID including Taklimakan desert) and Qaidam basin (35–39° N and 90–99° E, located in zone HIID1) with cumulative rainfall less than 200 mm, and abundant precipitation of about 1300 mm in southern Himalayas where Indian monsoon prevails. In addition, the strong contrast of precipitation pattern between northern and southern Himalayas identifies the orographic effect on precipitation (Barros et al., 2004). PERSIANN generates a large mass of precipitation over central and southern TP (mainly located in HIB and HIIAB), while TMPA and CMORPH do not (Xie et al., 2007). This feature has

been proved to be overestimation when compared to gauge measurements and will be discussed later.

3.2 Evaluation according to climate zones

We first examine how well satellite estimates detect rain events. A higher POD and ETS and a lower FAR are desirable. A threshold of 1.0 mm day-1 adopted by Dai (2006) for studying global daily precipitation is used here to discriminate whether rain occurs. TMPA and CMORPH show similar statistics: CMORPH has slightly larger POD with mean value around 0.70, and TMPA has slightly smaller FAR with mean value around 0.35 (Fig. 4a and b). However, plus symbols below whisker in Fig. 4a show that TMPA and CMORPH do not detect rain events well in several sites. Similarly, plus symbols above whisker in Fig. 4b show that TMPA and CMORPH tend to give false alarms in some sites. Of the three datasets, PERSIANN has the smallest POD and ETS and the largest FAR.

The spatial patterns of correlations and biases are illustrated in Figs. 5–6. Overall, PERSIANN, with smaller correlation and larger bias pattern, shows less correspondence with gauge measurements than TMPA and CMORPH. The indirect IR-precipitation relationship prevents PERSIANN from being more accurate than TMPA and CMORPH that rely more heavily on MW retrievals. For example, the correlation between brightness temperature and rainfall is weak if little water is available in air profiles. PERSIANN has difficulty addressing this condition since it is mainly based on brightness temperature without incorporating water availability in profiles. Serial correlations of TMPA and CMORPH exceed 0.6 for most gauges in Yalong River over southeastern TP (Fig. 5a and b). TMPA is unique of the three satellite datasets, in that a correction process is used against the monthly gauge data of GPCP to reduce the inherent bias in satellite-based precipitation estimates. As shown in Fig. 6a, TMPA exhibits lower serial biases compared to other satellite estimates, which is consistent with studies over other regions, e.g. Korea (Sohn et al., 2010), and Pacific Ocean (Sapiano

and Arkin, 2009). PERSIANN produces obvious overestimates over central and southern TP, while other two satellite datasets do not (Xie et al., 2007).

A specific comparison for every climate zone is applied to further understand the applicability of the three satellite products over different climate zones of TP. To assure the reliability of comparisons, only zones with at least 10 rain stations are selected. Statistics of every climate zone are averaged from gauges within the zones and shown in Table 3. Larger POD and ETS and lower FAR are observed over humid zones than over arid zones, and correlations present the similar situation. RMSE gradually increases from arid zones to humid zones, which may be due to higher amplitude of precipitation over more humid zones. Of the three datasets, TMPA exhibits the lowest biases over most zones, which is consistent with the bias pattern in Fig. 6. However, TMPA does not present similar advantages in RMSE, with larger RMSE than CMORPH over several zones, e.g. HIID1, HIIC1 and HIB. A possible explanation is that overall bias correction used in the TMPA product only allocate the overall bias to 3-hourly precipitation estimates, which only reduces the overall bias but does little to affect the magnitude of 3-hourly or daily random errors expressed by RMSE. PERSIANN, generally with smaller POD, ETS and correlations and larger FAR, bias and RMSE, does not present the same good statistics as the other two datasets.

3.3 Evaluation according to rainfall categories

Rainfall categories may have impact on the performance of satellite rainfall estimates. To explore different aspects of satellite products under different rainfall categories, rainfall is divided into four categories: 0–10, 10–25, 25–50, and > 50 mm. The mean bias for each category is calculated for TMPA, CMORPH and PERSIANN and the result is presented in Fig. 7. Overall, the three precipitation products generally tend to overestimate light rainfall (0–10 mmm) and underestimate moderate and heavy rainfall (> 10 mm). The underestimation for moderate and heavy rainfall increases. TMPA generally has higher performance than PERSIANN and CMORPH in different rainfall categories, showing the effect of incorporating gauge stations for correction. In general,

PERSIANN tends to produce higher positive bias for light rainfall and lower negative bias for moderate and heavy rainfall than TMPA and CMORPH. It is also interesting to note that the negative biases in semi-arid and arid zones is lower than those in semi-humid and humid zones, showing that the three satellite-based precipitation products are not good at estimating moderate and heavy rainfall in arid zones compared to humid zones. Although HIIC1 and HIIC2 are both located in semi-arid zones, PERSIANN has different performance in the two zones. PERSIANN generates slight overestimation for light rainfall in HIIC1 while heavy overestimation in HIIC2. Also, the negative bias of PERSIANN for moderate and heavy rainfall is much lower in HIIC1 than that in HIIC2. The difference may be attributed to elevation and will be further discussed in the next section.

3.4 Evaluation as a function of elevation

Following the rule used in the Sect. 3.2, only climate zones with at least 10 gauges are used to explore the bias-elevation relationship. The biases of the three satellite estimates as a function of elevation in seven selected zones are presented in Fig. 8. As shown in Fig. 8a and b, it is very interesting to note that the bias of PERSIANN in the zone HIB and HIIAB displays an increasing trend as elevation increases while TMPA and CMORPH present a decreasing trend. In Sect. 3.2 we have found that PERSIANN produces heavy overestimates over central and southern TP (approximately located in the zone HIB and HIIAB), so it is clear that the overestimation is more obvious at higher elevations. As seen in Fig. 8c, the bias of the three precipitation estimates in the zone VA does not show a strong dependence on the elevation while PERSIANN gives obvious underestimation in this area. Zone HIIC1 and HIIC2 are both characterized as sub-frigid and semi-arid zones. However, as shown in last section, PERSIANN tends to underestimate rainfall in HIIC1 but tends to overestimate rainfall in HIIC2 (Fig. 8d and e). Elevation may play an important role in the accuracy of PERSIANN since elevation considered in HIIC1 ranges from 1795 m to 3625 m, which is lower than that in HIIC2 (from 3277 m to 4826 m). In fact, Fig. 8 indicates that PERSIANN may

show underestimation at low elevations and overestimation at high elevations. To further prove it, Biases of PERSIANN at high and low elevations over TP are calculated, respectively and compared. 3500 m is roughly used as the division elevation, that is, elevations higher than 3500 m are defined as high elevations and vice versa. The bias of PERSIANN is 0.84 mm day^{-1} at high elevations and -0.64 mm day^{-1} at low elevations, showing that PERSIANN tends to produce systematic biases over TP. Although previous studies in northwestern Mexico and Ethiopia indicate that PERSIANN considerably underestimates rainfall at high elevations (Hong et al., 2007; Hirpa et al., 2010; Romilly and Gebremichael, 2011), high elevations in these studies should be generally treated as low elevations when compared with TP. For example, the highest elevation over northwestern Mexico is only about 3000 m.

As for CMORPH and TMPA, their biases present a decreasing trend as elevation increases in most climate zones except for HIIC2 and IID. However, the dependence of biases of CMORPH and TMPA on the elevation is not strong in most zones with statistical levels exceeding 5 % except for specific zones, that is, CMORPH in the HIB (Fig. 8a) and TMPA in the HIIAB and HIID1 (Fig. 8b and f).

4 Summary and conclusions

Several studies (e.g. Xie et al., 2007; Shen et al., 2010) were involved in the examination of the performance of satellite precipitation products over China. However, as far as we know, the examination over TP has not been specifically studied. We here provide a detailed evaluation of satellite precipitation at daily scale over TP with specific focus on the different climate zones and elevation. Three independently developed satellite precipitation products are compared against rain gauge measurements collected from CMA. A long validation period from May to October during 2004–2009 is chosen to avoid spurious results caused by spatial sampling or random errors. The major findings are summarized as follows.

1. With higher correlation and lower RMSE, TMPA and CMORPH show better performance than PERSIANN over TP.

2. Due to the correction process against monthly gauge measurements, TMPA displays the lowest biases. However, the process does little to affect the magnitude of 3-hourly or daily random errors expressed by RMSE compared to CMORPH and PERSIANN.

3. The three products show better agreement with rain gauge measurements in humid regions than that in arid regions.

4. The three precipitation products generally tend to overestimate light rainfall (0–10 mm) and underestimate moderate and heavy rainfall (> 10 mm).

5. PERSIANN produces obvious underestimation at low elevations and overestimation at high elevations. CMORPH and TMPA do not present strong bias-elevation relationships in most climate zones.

Given the sparse distribution of meteorological stations over TP, especially in regions at high elevations, satellite-based precipitation datasets provide an important way to map temporal and spatial pattern of precipitation. One goal of our study is to evaluate these satellite precipitation products with rain gauge observations before they are integrated into global circulation model to simulate global hydrometeorological processes, or into land surface model to understand regional hydrological processes. TMPA and CMORPH that depend heavily on MW data produce better precipitation estimates than PERSIANN that rely primarily on IR data. This result is consistent with other similar studies over different areas of the world, showing the advantages of incorporating MW data. There are two suggestions for the future work. First, the satellite-based datasets generate reasonable estimates of precipitation. However, a correction process based on topography, gauge observations or humidity at daily or finer time scale is valuable to relieve systematic biases to provide a more accurate precipitation input for global or regional modelling. Second, although our study covers most regions across TP, nearly

no gauges exist over northwestern TP where elevation is nearly higher than 4500m, so a closer precipitation observing network is needed in these regions for better comparison.

References

Barros, A. P., Kim, G., Williams, E., and Nesbitt, S. W.: Probing orographic controls in the Himalayas during the monsoon using satellite imagery, Nat. Hazards Earth Syst. Sci., 4, 29–51, doi:10.5194/nhess-4-29-2004, 2004.

Bell, T. L. and Kundu, P. K.: Comparing satellite rainfall estimates with rain gauge data: Optimal strategies suggested by a spectral model, J. Geophys. Res.-Atmos., 108, 4121, doi:10.1029/2002jd002641, 2003.

Bowman, K. P.: Comparison of TRMM precipitation retrievals with rain gauge data from ocean buoys, J. Climate, 18, 178–190, 2005.

Ciach, G. J. and Krajewski, W. F.: On the estimation of radar rainfall error variance, Adv. Water Resour., 22, 585–595, doi:10.1016/s0309-1708(98)00043-8, 1999.

Dai, A.: Precipitation characteristics in eighteen coupled climate models, J. Climate, 19, 4605–4630, doi:10.1175/jcli3884.1, 2006.

Demirtas, M., Nance, L., Bernardet, L., Lin, Y., Chuang, H. Y., Loughe, A., Mahoney, J., Gall, R., and Koch, S.: The developmental testbed center verification system, http://www.mmm.ucar.edu/wrf/users/workshops/WS2005/abstracts/Session3/23-DEMIRTAS.pdf (last access: 11 July 2012), June 2005.

Dinku, T., Chidzambwa, S., Ceccato, P., Connor, S. J., and Ropelewski, C. F.: Validation of high-resolution satellite rainfall products over complex terrain, Int. J. Remote Sens., 29, 4097-4110, doi:10.1080/01431160701772526, 2008.

Title Page

Abstract | Introduction

Conclusions | References

Tables | Figures

|◄ | ►|

◄ | ►

Back | Close

Full Screen / Esc

Printer-friendly Version

Interactive Discussion

Ebert, E. E., Janowiak, J. E., and Kidd, C.: Comparison of near-real-time precipitation estimates from satellite observations and numerical models, B. Am. Meteorol. Soc., 88, 47–64, doi:10.1175/bams-88-1-47, 2007.

Gottschalck, J., Meng, J., Rodell, M., and Houser, P.: Analysis of multiple precipitation products and preliminary assessment of their impact on global land data assimilation system land surface states, J. Hydrometeorol., 6, 573–598, 2005.

Hirpa, F. A., Gebremichael, M., and Hopson, T.: Evaluation of High-Resolution Satellite Precipitation Products over Very Complex Terrain in Ethiopia, J. Appl. Meteorol. Clim., 49, 1044–1051, doi:10.1175/2009jamc2298.1, 2010.

Hong, Y., Hsu, K. L., Sorooshian, S., and Gao, X. G.: Precipitation Estimation from Remotely Sensed Imagery using an Artificial Neural Network Cloud Classification System, J. Appl. Meteorol., 43, 1834-1852, 2004.

Hong, Y., Gochis, D., Cheng, J.-T., Hsu, K.-L., and Sorooshian, S.: Evaluation of PERSIANN-CCS Rainfall Measurement Using the NAME Event Rain Gauge Network, J. Hydrometeorol., 8, 469–482, doi:10.1175/jhm574.1, 2007.

Hsu, K. L., Gupta, H. V., Gao, X. G., and Sorooshian, S.: Estimation of physical variables from multichannel remotely sensed imagery using a neural network: Application to rainfall estimation, Water Resour. Res., 35, 1605–1618, 1999.

Huffman, G. J., Adler, R. F., Arkin, P., Chang, A., Ferraro, R., Gruber, A., Janowiak, J., Mc-Nab, A., Rudolf, B., and Schneider, U.: The Global Precipitation Climatology Project (GPCP) Combined Precipitation Dataset, B. Am. Meteorol. Soc., 78, 5–20, 1997.

Huffman, G. J., Bolvin, D. T., Nelkin, E. J., Wolff, D. B., Adler, R. F., Gu, G., Hong, Y., Bowman, K. P., and Stocker, E. F.: The TRMM Multisatellite Precipitation Analysis (TMPA): Quasi-Global, Multiyear, Combined-Sensor Precipitation Estimates at Fine Scales, J. Hydrometeorol., 8, 38–55, doi:10.1175/jhm560.1, 2007.

Joyce, R. J., Janowiak, J. E., Arkin, P. A., and Xie, P. P.: CMORPH: A method that produces global precipitation estimates from passive microwave and infrared data at high spatial and temporal resolution, J. Hydrometeorol., 5, 487–503, 2004.

Legates, D. R. and Willmott, C. J.: Mean seasonal and spatial variability in gauge-corrected, global precipitation, Int. J. Climatol., 10, 111–127, 1990.

Pan, M., Li, H., and Wood, E.: Assessing the skill of satellite-based precipitation estimates in hydrologic applications, Water Resour. Res., 46, W09535, doi:10.1029/2009wr008290, 2010.

Title Page

Abstract	Introduction
Conclusions	References
Tables	Figures

|◄ | ►|

◄ | ►

Back | Close

Full Screen / Esc

Printer-friendly Version

Interactive Discussion

Romilly, T. G. and Gebremichael, M.: Evaluation of satellite rainfall estimates over Ethiopian river basins, Hydrol. Earth Syst. Sci., 15, 1505–1514, doi:10.5194/hess-15-1505-2011, 2011.

Sapiano, M. R. P. and Arkin, P. A.: An Intercomparison and Validation of High-Resolution Satellite Precipitation Estimates with 3-Hourly Gauge Data, J. Hydrometeorol., 10, 149–166, doi:10.1175/2008jhm1052.1, 2009.

Schaefer, J. T.: The critical success index as an indicator of warning skill, Weather Forecast., 5, 570–575, doi:10.1175/1520-0434(1990)005<0570:tcsiaa>2.0.co;2, 1990.

Shen, Y., Xiong, A., Wang, Y., and Xie, P.: Performance of high-resolution satellite precipitation products over China, J. Geophys. Res., 115, D02114, doi:10.1029/2009jd012097, 2010.

Shi, X. Y., Wang, Y. Q., and Xu, X. D.: Effect of mesoscale topography over the Tibetan Plateau on summer precipitation in China: A regional model study, Geophys. Res. Lett., 35, L19707, doi:10.1029/2008gl034740, 2008.

Sohn, B. J., Han, H.-J., and Seo, E.-K.: Validation of Satellite-Based High-Resolution Rainfall Products over the Korean Peninsula Using Data from a Dense Rain Gauge Network, J. Appl. Meteorol. Clim., 49, 701–714, doi:10.1175/2009jamc2266.1, 2010.

Sorooshian, S., Hsu, K. L., Gao, X., Gupta, H. V., Imam, B., and Braithwaite, D.: Evaluation of PERSIANN system satellite-based estimates of tropical rainfall, B. Am. Meteorol. Soc., 81, 2035–2046, 2000.

Sorooshian, S., AghaKouchak, A., Arkin, P., Eylander, J., Foufoula-Georgiou, E., Harmon, R., Hendrickx, J. M. H., Imam, B., Kuligowski, R., Skahill, B., and Skofronick-Jackson, G.: Advanced concepts on remote sensing of precipitation at multiple scales, B. Am. Meteorol. Soc., 92, 1353–1357, doi:10.1175/2011bams3158.1, 2011.

Sun, H. L. and Zheng, D.: The formation, evolution and development of Qinghai-Tibet Plateau, Guangdong Science and Technology Press, Guangdong, 350 pp., 1999.

Xie, P., Chen, M., Yang, S., Yatagai, A., Hayasaka, T., Fukushima, Y., and Liu, C.: A Gauge-Based Analysis of Daily Precipitation over East Asia, J. Hydrometeorol., 8, 607–626, doi:10.1175/jhm583.1, 2007.

Yanai, M. H., Li, C. F., and Song, Z. S.: Seasonal heating of the tibetan plateau and its effects on the evolution of the asian summer monsoon, J. Meteorol. Soc. Jpn., 70, 319–351, 1992.

Yeh, D. Z. and Gao, Y. X.: The Meteorology of the Tibetan Plateau, Science Press, Beijing, 278 pp., 1979.

Evaluation of high-resolution satellite precipitation products

Y. C. Gao and M. F. Liu

Title Page

Abstract | Introduction

Conclusions | References

Tables | Figures

|◄ | ►|

◄ | ►

Back | Close

Full Screen / Esc

Printer-friendly Version

Interactive Discussion

Yin, Z.-Y., Zhang, X., Liu, X., Colella, M., and Chen, X.: An Assessment of the Biases of Satellite Rainfall Estimates over the Tibetan Plateau and Correction Methods Based on Topographic Analysis, J. Hydrometeorol., 9, 301–326, doi:10.1175/2007jhm903.1, 2008.

Evaluation of high-resolution satellite precipitation products

Y. C. Gao and M. F. Liu

Title Page

Abstract | Introduction

Conclusions | References

Tables | Figures

◄ | ►

◄ | ►

Back | Close

Full Screen / Esc

Printer-friendly Version

Interactive Discussion

Table 1. The indices used to divide TP into climate zones. Note that denotes annual evapotranspiration (mm), and denotes annual precipitation (Sun and Zheng, 1999).

Indices	Number of days	Indices	Dryness	Annual precipitation (mm)
Subtropical	> 180	Humid	< 1.0	> 800
Warm-temperate	141–180	Semi-humid	1.0–1.5	500–800
Temperate	51–140	Semi-arid	1.6–5.0	200–499
Sub frigid	1–50	Arid	5.1–15	50–199
Frigid	0	–	–	–

Table 2. Characteristics of the climate zones. The rainy season precipitation here refers to six months from May to October and is calculated as the median of TMPA, CMORPH and PERSIANN estimates.

Zones	Mean elevation (m)	Rainy season precipitation (mm)	Number of rain gauges	Zones	Mean elevation (m)	Rainy season precipitation (mm)	Number of rain gauges
HOD	4363	119	3	HIID2	4949	134	1
HIB	4499	505	15	IID	1507	155	13
HIC	4870	243	7	IIID	1224	96	9
HIIAB	4145	621	30	IVA	1849	474	1
HIIC1	3239	363	22	VA	1699	684	33
HIIC2	4920	332	18	VIA	1642	705	2
HIID1	3347	123	10	VIIA	2552	616	2

Title Page

Abstract | Introduction

Conclusions | References

Tables | Figures

|◄ | ►|

◄ | ►

Back | Close

Full Screen / Esc

Printer-friendly Version

Interactive Discussion

Table 3. Evaluation statistics (calculated at daily time scale) of rain gauge measurements verse satellite estimates over different zones.

Indices	Zone name	Satellite datasets	POD	FAR	ETS	Correlation	Bias	RMSE
Semi-humid	HIB	TMPA	0.67	0.25	0.30	0.50	−0.32	5.19
		CMORPH	0.75	0.27	0.31	0.57	−0.07	4.56
		PERSIANN	0.69	0.31	0.24	0.41	0.49	6.16
Humid or semi-humid	HIIAB	TMPA	0.76	0.28	0.34	0.59	0.00	5.28
		CMORPH	0.78	0.31	0.33	0.62	0.14	4.98
		PERSIANN	0.69	0.30	0.29	0.48	0.45	6.56
Humid	VA	TMPA	0.74	0.27	0.37	0.67	−0.03	8.93
		CMORPH	0.73	0.24	0.39	0.67	−0.89	8.60
		PERSIANN	0.54	0.29	0.24	0.46	−1.76	10.36
Semi-arid	HIIC1	TMPA	0.63	0.34	0.29	0.55	−0.22	4.93
		CMORPH	0.71	0.36	0.31	0.59	−0.29	4.40
		PERSIANN	0.51	0.39	0.21	0.36	−0.74	5.67
Semi-arid	HIIC2	TMPA	0.69	0.35	0.34	0.54	−0.05	4.67
		CMORPH	0.66	0.39	0.29	0.48	−0.43	4.40
		PERSIANN	0.75	0.39	0.33	0.53	1.33	6.10
Arid	HIID1	TMPA	0.37	0.58	0.18	0.32	−0.15	2.63
		CMORPH	0.46	0.63	0.18	0.40	−0.19	2.12
		PERSIANN	0.49	0.71	0.14	0.27	0.14	2.74
Arid	IID	TMPA	0.59	0.48	0.30	0.50	0.15	3.16
		CMORPH	0.70	0.50	0.33	0.51	0.19	2.92
		PERSIANN	0.48	0.59	0.20	0.29	−0.06	3.43
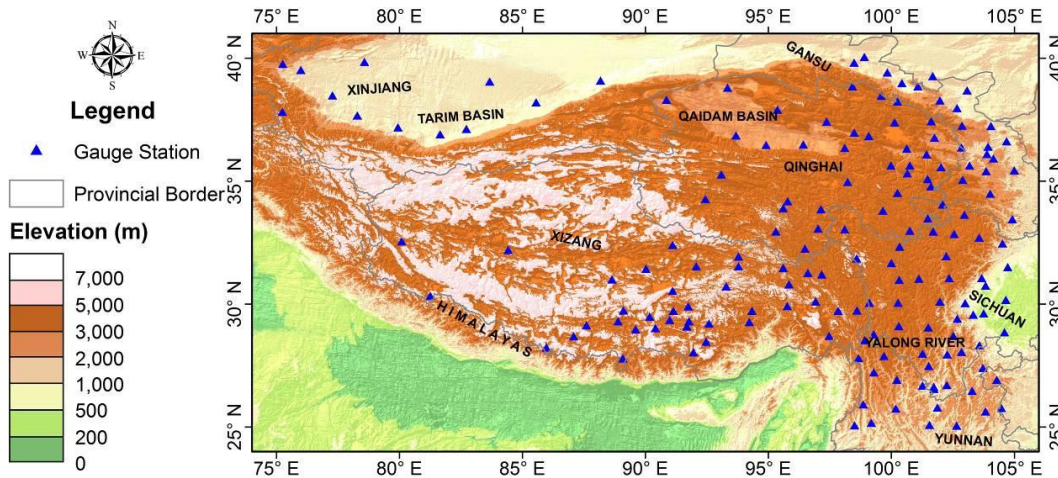
Fig. 1. Rain gauge network consisted of 166 stations used in our study and the elevation pattern over the entire Tibetan Plateau and its peripheral regions.
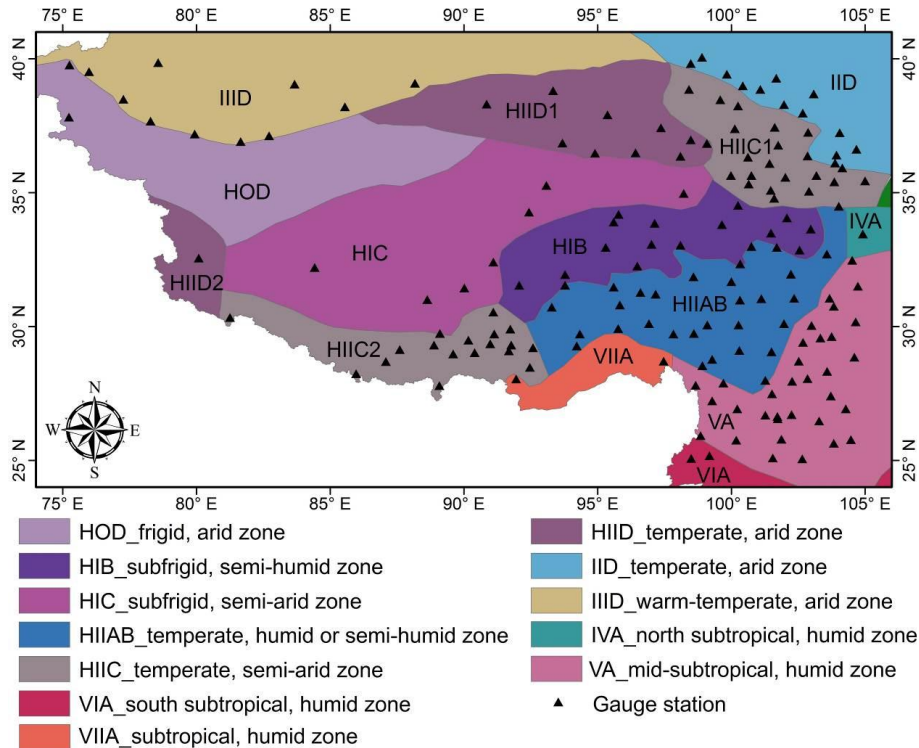
Fig. 2. The climate zones over Tibetan Plateau and its peripheral areas and the 166 rain gauges.
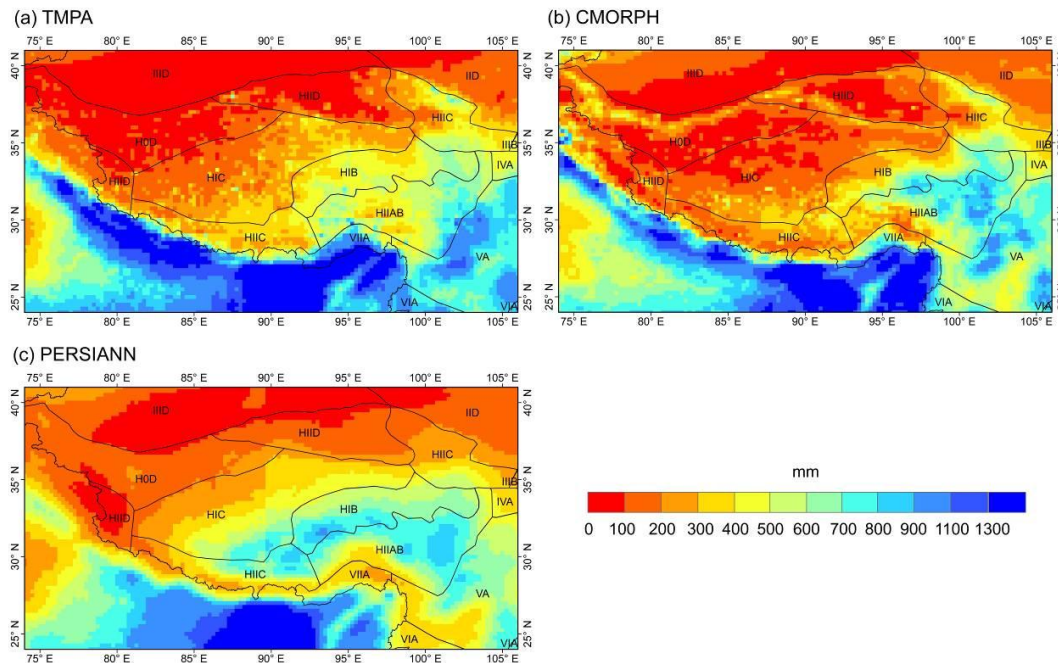
Fig. 3. The six-year mean rainy season precipitation during 2004–2009 for **(a)** TMPA; **(b)** CMORPH; and **(c)** PERSIANN.
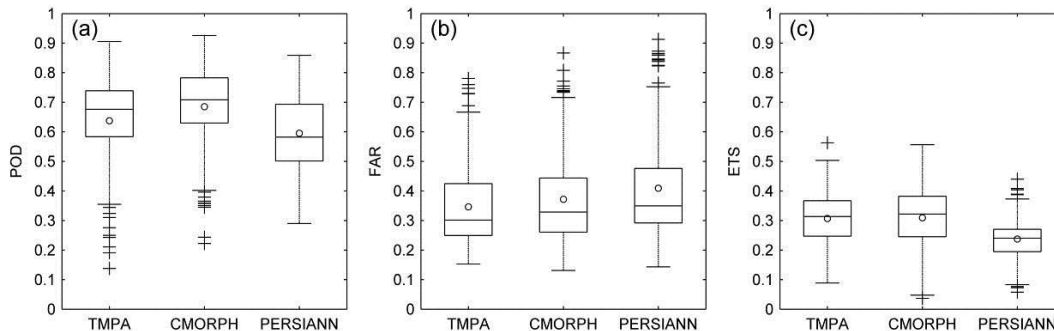
Fig. 4. Box plots of contingency table statistics for **(a)** POD, **(b)** FAR and **(c)** ETS. The circle represents the mean value. Each box ranges from the lower quartile (25th) to upper quartile (75th). The median is presented by the middle line in the box. The whiskers extend out to largest and smallest values within 1.5 times the interquartile range (difference between the 75th and 25th percentiles). The plus represents the points beyond the whiskers.

Title Page

Abstract | Introduction

Conclusions | References

Tables | Figures

◄ | ►|

◄ | ►

Back | Close

Full Screen / Esc

Printer-friendly Version

Interactive Discussion
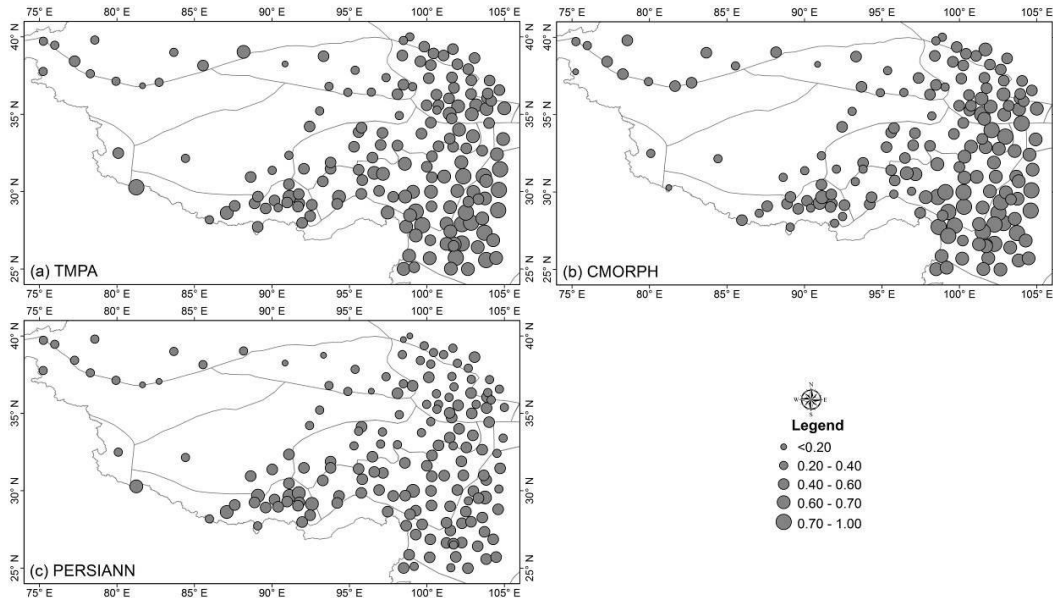
Fig. 5. The spatial pattern of correlations between gauge-based daily precipitation and that derived from satellite products from May to October during 2004–2009. Note that every circle depicts a gauge station.
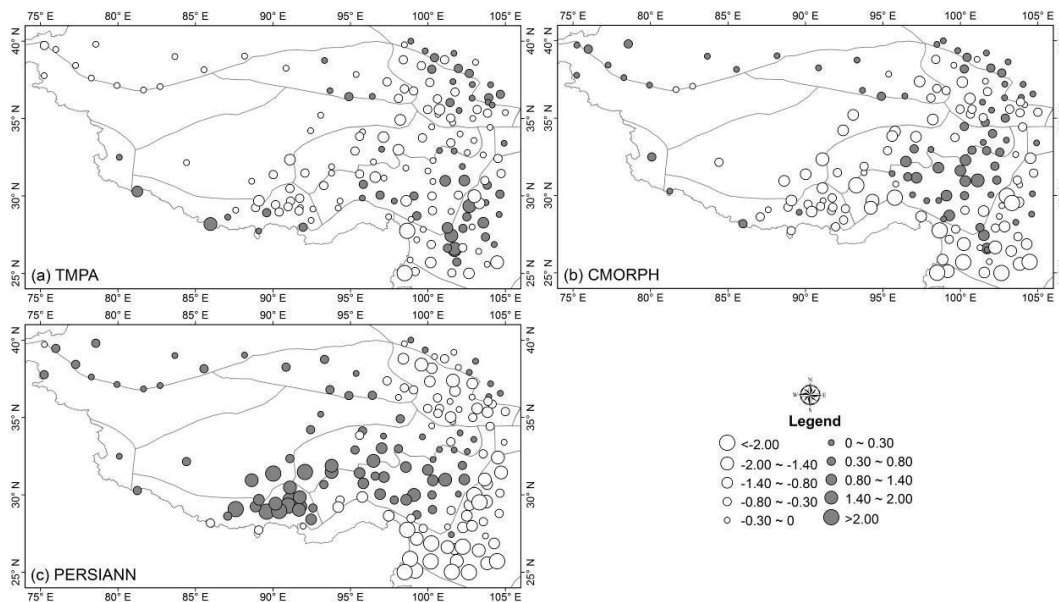
Fig. 6. The spatial pattern of biases $= S - G$ (mm day^{-1}) between gauge-based daily precipitation and that derived from satellite products from May to October during 2004–2009.
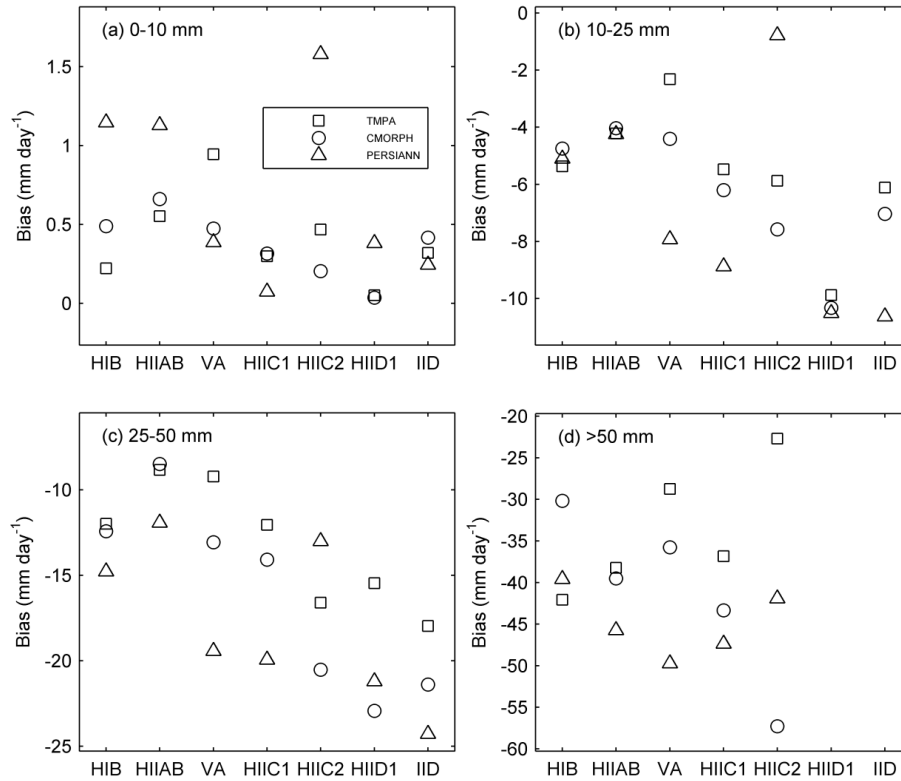
Fig. 7. Bias of the three satellite-based precipitation products for different rainfall categories.
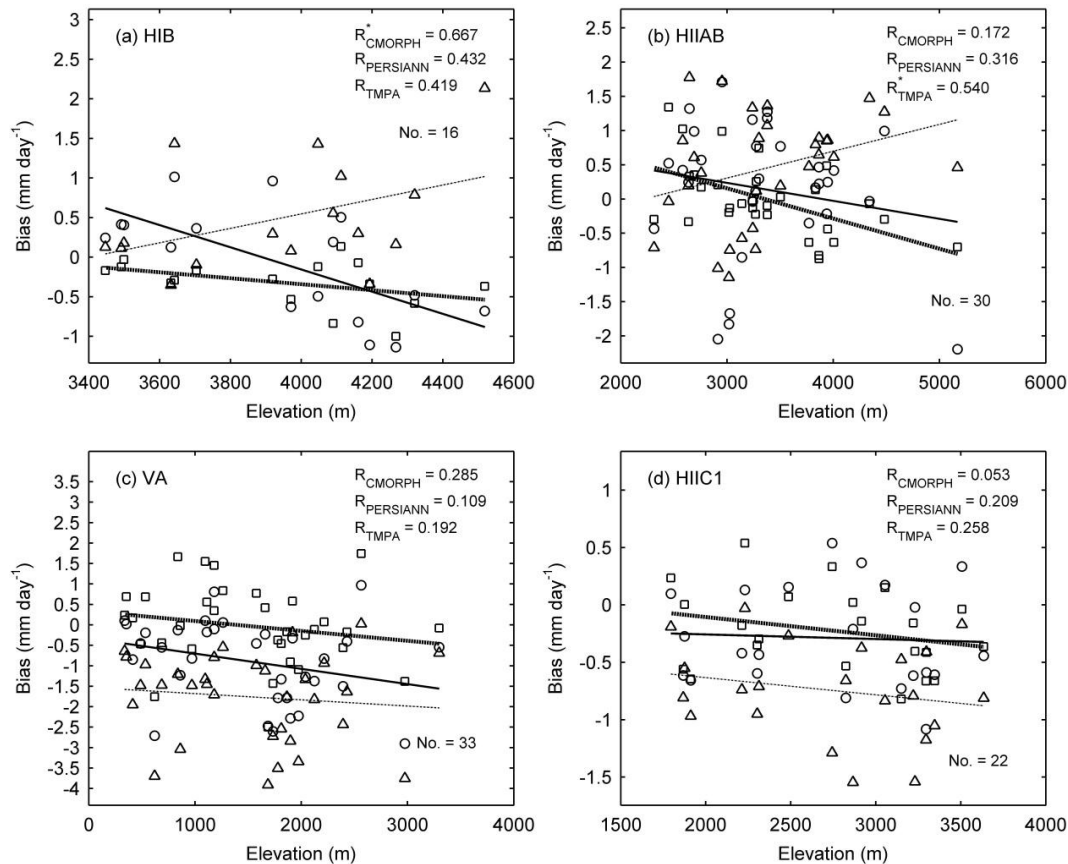
Fig. 8. See caption on next page.

Title Page

Abstract   Introduction

Conclusions   References

Tables   Figures

⏮   ⏭

◀   ▶

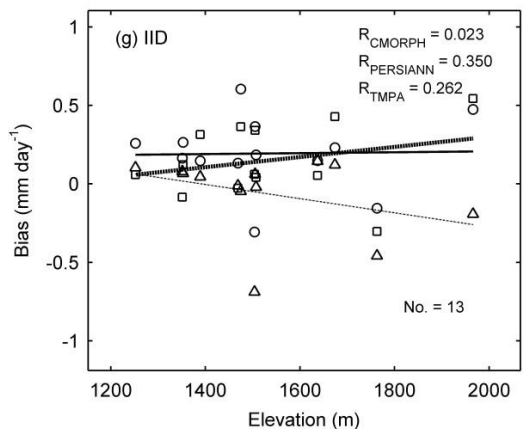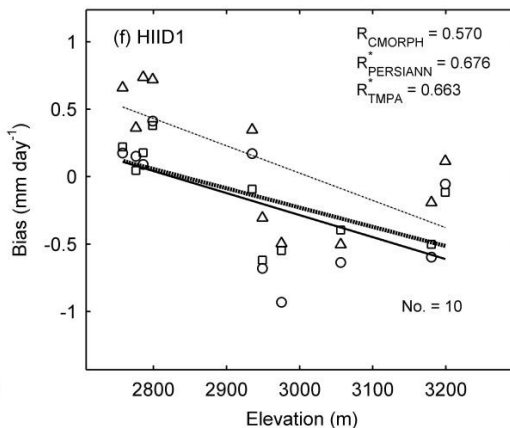Back   Close

Full Screen / Esc
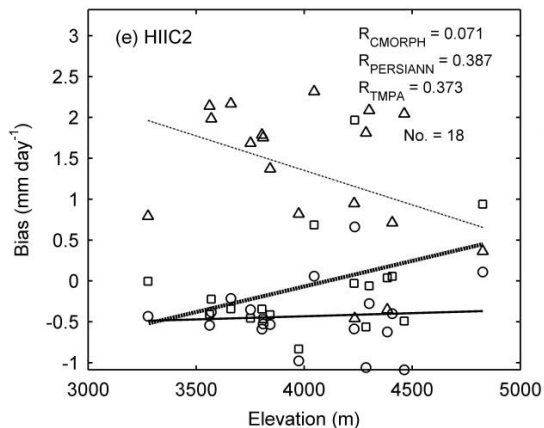
Printer-friendly Version

Interactive Discussion
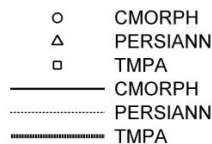
Fig. 8. The relationship between bias and elevation in seven climate zones. Lines denote the least squares regression lines. R and R^* denote correlation with statistical level exceeding and less than 0.05, respectively. No. denotes the number of gauges used.

Title Page

Abstract | Introduction

Conclusions | References

Tables | Figures

|◄ | ►|

◄ | ►

Back | Close

Full Screen / Esc

Printer-friendly Version

Interactive Discussion